

Tunable Microstructured Surface-Enhanced Raman Scattering Substrates via Electrohydrodynamic Lithography

Sumeet Mahajan*,†,‡ Tanya Hutter,†,¶ Ullrich Steiner,† and Pola Goldberg Oppenheimer*,§

†Department of Physics, Cavendish Laboratory, University of Cambridge, J J Thomson Avenue, Cambridge CB30HE, United Kingdom

‡Institute for Life Sciences, Highfield Campus, University of Southampton, Southampton SO17 1BJ, United Kingdom

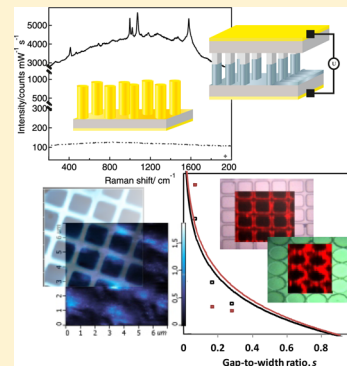
¶Department of Chemistry, University of Cambridge, Cambridge CB2 1EW, United Kingdom

§School of Chemical Engineering, University of Birmingham, Edgbaston B15 2TT, United Kingdom

Supporting Information

ABSTRACT: Readily fine-tuned structures are an important requirement for the optimization of surface-enhanced Raman scattering (SERS) to obtain the highest enhancements. Here, a lateral modulation of an electric field applied to a dielectric interface enables the rapid replication of nearly any topographic morphology with micrometer resolution by electrohydrodynamic lithography (EHL). Gold-covered periodic EHL-generated arrays yielded the reproducible enhancement of adsorbed SERS-active molecules. Periodic arrays of micropillars with square and circular cross sections give rise to the effective coupling of surface plasmon modes, which generate enhanced SERS signals. The overall enhancement factors depend on the geometry of the gold-coated structures, and intriguingly, a strong correlation is found with the gap-to-width ratio of the square pillar morphology. A numerical simulation of the EHL-based SERS substrates is consistent with this dependence. The EHL surface architectures can be easily tailored at micrometer-to-submicrometer dimensions, allowing the fabrication of reliably engineered and cost-effective highly sensitive SERS substrates.

SECTION: Plasmonics, Optical Materials, and Hard Matter



Surface-enhanced Raman spectroscopy (SERS) is a highly sensitive detection method for molecules. It is based on the optical excitation of localized surface plasmon resonances (LSPRs), which give rise to intense local electric fields in coinage metal structures. The coupling of this surface field to excitations of adsorbed molecules causes an enhancement of Raman scattering by many orders of magnitude.^{1,2} This leads to the requirement for the rational design and fabrication of surface structures to effectively enhance local electromagnetic fields for utilization of SERS in a range of applications, in particular, in medical diagnostics.^{3–7} Nanosphere self-assembly and standard lithographic techniques enable the manufacture of large-area (irregular and ordered) SERS-active surfaces with intense electromagnetic “hot spots” that yield high SERS enhancement.^{8–13} They can be, however, inconsistent in terms of the measured signal, and repeatability between different, although seemingly identical, substrates is difficult to achieve.^{14,15} Electron beam and photolithography are able to create sophisticated surface patterns for SERS,^{10,16} but they typically require expensive and cumbersome multistep fabrication processes, which limit the scalability of the resulting structures. Alternative routes for multiscale structures include self-assembly or chemical processes,¹² but the precise control of features and prevention of defects remain a challenge, particularly in the submicrometer regime. The variable signal

enhancement measured across single as well as (outwardly) identical SERS substrates further exacerbates the drawbacks of the current manufacturing processes. Moreover, while the advantages of periodically structured substrates for SERS have been demonstrated to enable improved enhancement,¹⁶ reproducible and versatile platforms that allow the easy adjustment of structural parameters are still difficult to accomplish. These hindrances underline the constant need for versatile, cost-effective, and straightforward methods to develop tunable three-dimensional structures that exhibit consistent and reliable signal enhancement across the surface.

Here, we report an electrohydrodynamic lithography (EHL) approach that addresses certain setbacks described above while enabling the tuning of the LSPRs by generating a range of versatile micrometer-sized structures with design geometries and periodicities. EHL harnesses instabilities in thin films induced by a *lateral* electric field variation, which causes the break-up of a thin polymer film and guides the material into design structures, allowing a one-step patterning of a broad range of architectures. Thus, EHL provides an important stepping stone toward generating reproducible, three-dimen-

Received: September 2, 2013

Accepted: November 19, 2013

Published: November 19, 2013

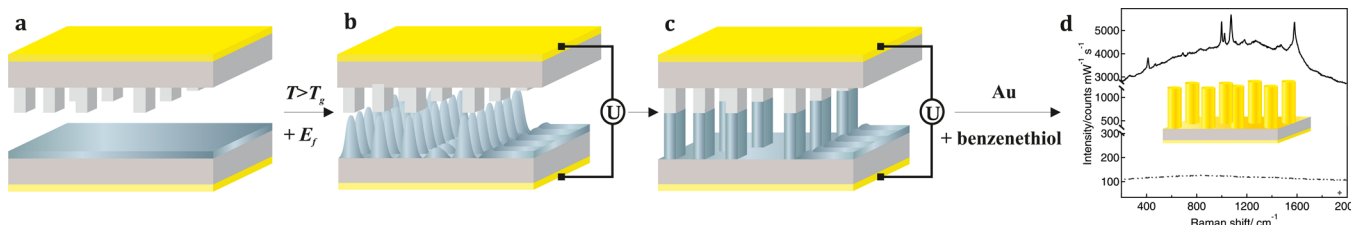


Figure 1. EHL pattern generation in a capacitor assembly is (a) triggered by the liquefaction of a polymer film and the amplification of instability by (b) the application of a voltage U across the two capacitor plates, giving rise to an electric field E_f that varies laterally across the device. The reduced distance between downward-protruding parts of the structured electrode and the film locally enhances the electric field, triggering film destabilization and focusing the electrohydrodynamic instability toward these protrusions. This yields a pillar pattern (c) spanning the capacitor gap at the locations of the smallest interelectrode distances, generating a replica of the upper electrode. (d) Coating the generated structures with a thin gold layer (inset) yields a SERS platform with enhancement factors up to 10^7 relative to a flat gold-coated substrate.

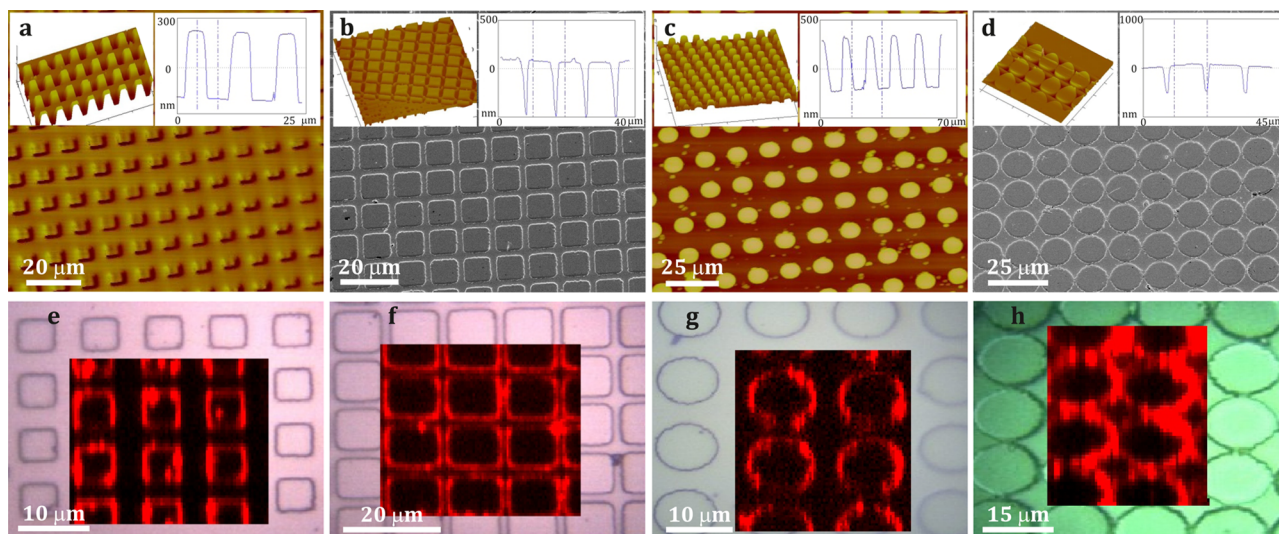


Figure 2. (a–d) AFM and SEM images of high-fidelity EHL-generated patterns. Periodic square prism-like arrays of (a) height $h = 500 \text{ nm}$, width $d = 5 \mu\text{m}$, and periodicity $\lambda = 5 \mu\text{m}$ and (b) $h = 500 \text{ nm}$, $d = 10 \mu\text{m}$, and $\lambda = 2.8 \mu\text{m}$. Cylindrical pillar arrays with (c) $h = 500 \text{ nm}$, $d = 8 \mu\text{m}$, and $\lambda = 8 \mu\text{m}$ and (d) $h = 500 \text{ nm}$, $d = 13 \mu\text{m}$, and $\lambda = 1 \mu\text{m}$. The corresponding three-dimensional AFM representations are shown in the insets. (e–h) Raman emission maps of the benzenethiol peak at 1070 cm^{-1} overlaid over an optical image of each patterned area, revealing the location of SERS enhancement localized at the perimeter edge of these structures.

sional, and long-range periodic SERS-active architectures. The predesigned top electrode is highly reusable by employing self-assembled monolayer deposition, which is a standard way to reduce the surface energy while facilitating a nondestructive release of chemical and biological substances from metallic electrodes and can be hugely advantageous for calibration and long-term reusability. After coating with a plasmon-active metal such as gold, this provides versatile SERS-active substrates that overcome some of the typical drawbacks of other fabrication methods, which exhibit repeatable SERS enhancement from easily detectable structures under the optical microscope. Interestingly, however, in contrast to the *submicrometer* EHD-generated SERS pillars (with an only local symmetry) where *each* of the individual structural units yields a considerable SERS enhancement arising almost exclusively from a single column,¹³ a different behavior is observed for the micrometer-size EHL-generated topographic morphologies. Depending on the structure and interstructure spacing, certain periodic arrays exhibited SERS enhancement either at their perimeter or in the area between the structures. Further, polarization-dependent SERS is detected at the interstitial locations of the periodic structures. The EHL technique offers a great variability of structural features by the independent control of several

parameters in a robust fashion, generating high-fidelity uniform patterns across large substrate areas. It thus provides a complementary platform for the reliable manufacture of substrates with consistent SERS enhancements. The tuning of plasmon resonances is further accomplished by controlling the dimensions, geometry, and aspect ratio of the EHL-generated pillar arrays. This tunability allows the design of SERS substrates that generate strong localized electromagnetic fields at optical wavelengths that are required for the optimum SERS excitation by different laser sources.

The EHL method makes use of a capacitor device that includes a polymer-film-covered electrode opposed by a reusable upper electrode with a topographic design pattern (Figure 1a; see the Experimental Section for further details). For an externally applied electric field, the topographic pattern is an equipotential surface. The variation in the interelectrode spacing d therefore results in a lateral inhomogeneous field. The electric field in the capacitor device gives rise to an instability in the film that is triggered at the location of smallest d . The growth of this instability is further focused in the direction of the highest electric field (i.e., smallest d) (Figure 1b). The instability is thereby guided toward the protruding patterns of the top mask, forming a positive replica (Figure 1c). The final

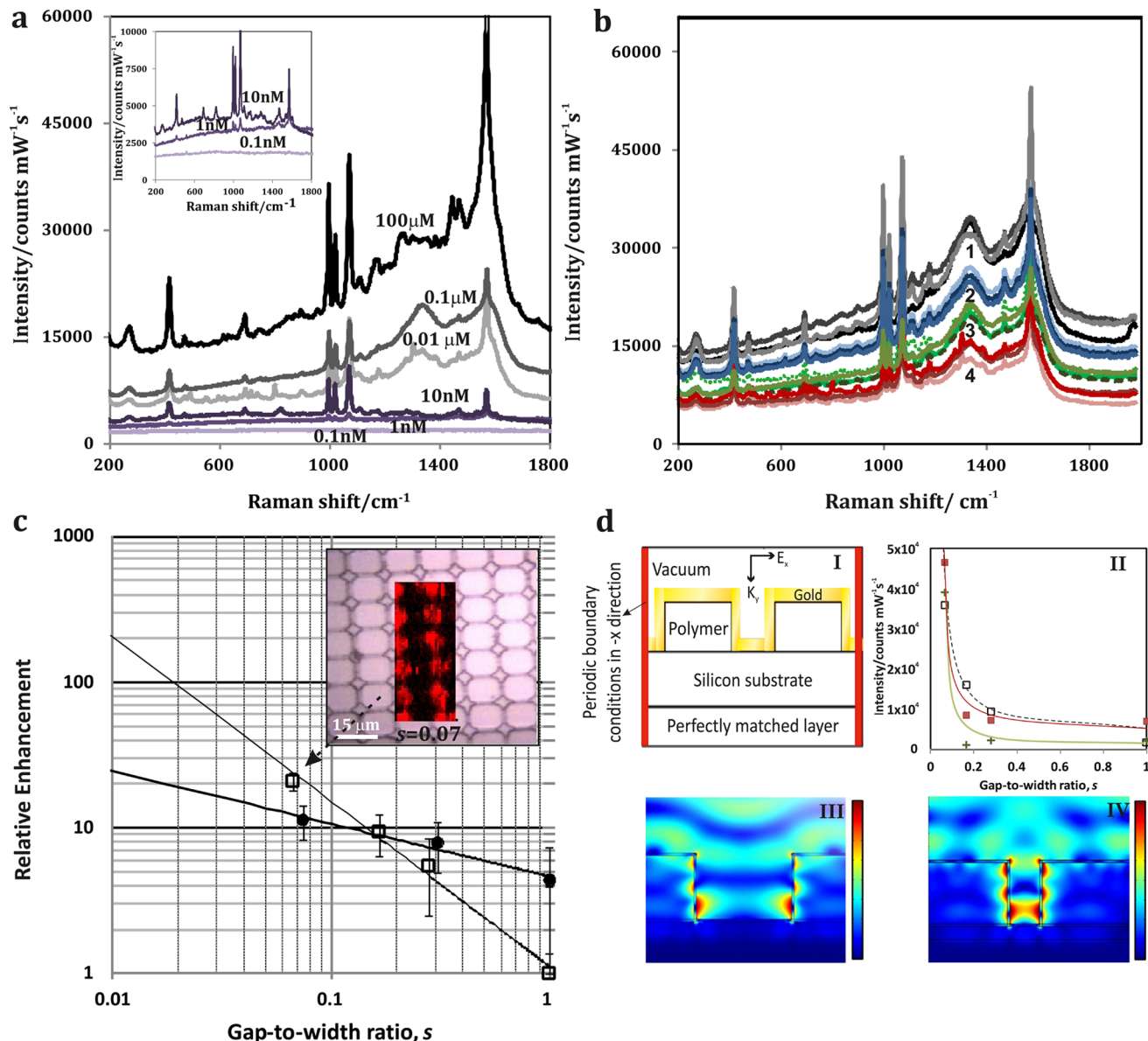


Figure 3. (a) The detection sensitivity of interstitial diamond-like (inverted squares) structure (shown in the inset of c) of recorded SERS spectra at $100 \mu\text{M}$ – 0.1nM concentrations at identical integration times and laser power (10s , 10mW). An enlarged view of the 10 , 1 , and 0.1nM spectra shows trace detection of sub-nM concentrations. (b) Representative SERS spectra of benzenethiol molecules on four periodic substrates across 3 – 4 random areas on each substrate with a 633 nm laser and a 10 s integration time, demonstrating reliable signal and substrate reproducibility. (c) Relative SERS enhancement of the 1070 cm^{-1} peak for circular (filled circles) and square (empty squares) pillar arrays with varying gap-to-width ratios. (Inset) Square-shaped pillars ($s = 0.07$) exhibit signals arising from the gap between the pillars. (d) Schematic illustration of the simulated 2D model, yielding (I), a consistent dependence of the SERS intensity with (black crosses) and without (red filled squares) periodic boundary conditions compared to the experiment (black empty squares). Lines are guides to the eye. 2D near-field simulations of the electric field distribution for (III) large and (IV) small values of s . Both the confined and scattered field components are visible.

height of the structure is determined by the plate spacing. The EHL technique is able to replicate a wide range of patterns with high-fidelity and micro-to-nanometric lateral length scales. The EHL-generated structures subsequently covered with a plasmon-active metal, gold in this case, effectively enhance local electromagnetic fields upon laser irradiation, leading to high SERS enhancements (Figure 1d).

EHL replication allows the replication of templates with a large range of feature sizes. Figure 2a–d shows atomic force microscopy (AFM) and scanning electron microscopy (SEM) images of representative EHL patterned arrays with various geometries, square prisms (Figure 2a and b) and cylindrical

pillars (Figures 2c and d) with feature sizes of 1.5 – $13.5 \mu\text{m}$ and interstructure spacings of 0.25 – $8 \mu\text{m}$. These patterns were evaluated in terms of their effectiveness to enhance the SERS signal intensities of the benzenethiol model molecule.

To this end, a 20 nm -thick gold layer was deposited onto the various polymer structures (see the Supporting Information (SI) for details) and coated with a monolayer of benzenethiol by dipping them into a 10 mM solution for 4 h . The Raman emission from the structured surfaces was acquired under identical conditions, and the resulting SERS maps were superimposed over the optical images, as shown in Figure 2e–h. Although the gold coating had a homogeneous thickness,

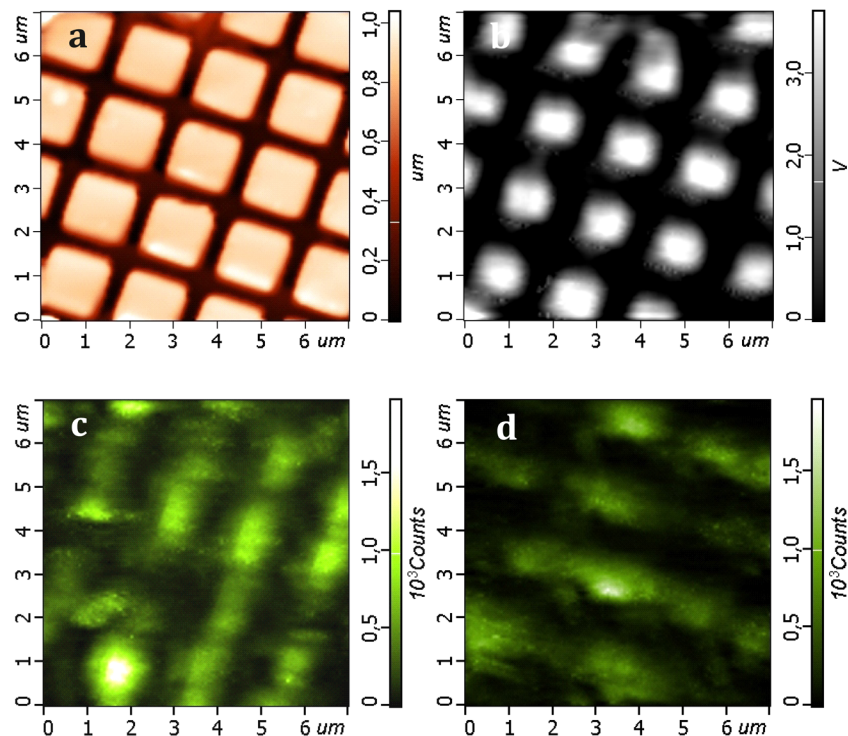


Figure 4. AFM tapping mode topography (a) and confocal image of the backscattered Rayleigh signal at 633 nm. (b) Raman scattering obtained simultaneously with NT-MDT VIT_P cantilevers, with a laser spot focused on the tip apex, confirming the SERS activity of the EHL-generated structure. Raman mapping with (c) vertically and (d) horizontally polarized excitation. The polarized Raman images were obtained by mapping the Raman intensity of the integrated 1000–1200 cm^{-1} peaks of benzenethiol adsorbed on a patterned Au substrate.

the SERS enhancement at 1070 cm^{-1} (bright) was observed only at the perimeter of these surface protrusions with no signal emanating from the flat sputtered gold on top or between the structures in Figure 2e–h. The flat part of the samples with just the sputtered gold layer as well as reference samples with just gold coated on polymer surfaces did not give any SERS signals. This confirms that EHL-patterned structures are indeed solely responsible for any observed SERS enhancements.

The characteristic Raman peaks of benzenethiol at 1000, 1070, and 1575 cm^{-1} (ref 17) were readily detected in the spectra acquired from the EHL-patterned substrates (Figure 3). Sensitivity and reproducibility are important figures of merit to quantify the SERS enhancement arising from topographically structured substrates. To address the sensitivity of the detection, we tested the SERS performance of the square array morphology, which gave the highest enhancement (Figure 3a; see the Experimental Section for the calculation of the enhancement factor) using different concentrations of benzenethiol in ethanolic solution. The SERS enhancement decreases with increasing dilution, yielding a detection limit of 1 nM (Figure 3a). A SERS trace of the molecule is even clearly visible at concentrations below 1 nM, as shown in the enlarged view of the SERS spectra in the inset of Figure 3a. This shows that very low solution concentrations can be detected with the EHL-fabricated SERS substrates of Figure 2. To evaluate the SERS signal reproducibility, we tested four EHL-generated substrates by examining several different areas across each surface under identical experimental conditions using 10 mM benzenethiol as the analyte. Good signal reproducibility was obtained from each substrate (four substrates tested, 3–4 areas on each substrate), yielding similar relative peak intensities (Figure 3b). The differences are more in the background than

the actual SERS peak. Also, SERS spectra taken from different locations across each sample were very similar, demonstrating good consistency. Variations of less than 10% standard deviation with an average variation of 3% in terms of the relative peak intensities were determined. Thus, our substrates offer uniform periodic structures with reproducible SERS enhancement made by the cost-effective EHL.

While all EHL-generated substrates yielded high Raman enhancements, the location of the SERS signal varied. Depending on the structure and interstructure spacing, square-shaped pillar arrays exhibited SERS enhancement either at their perimeter (Figure 2e–f) or in the area between the pillars (Figure 3c). A systematic analysis reveals that the relative enhancement correlates directly with the gap-to-width ratio s , highlighting a key parameter for the design of optimized EHL-generated SERS-active surfaces. Compared to a square pillar array with $s = 1$, the highest relative enhancement was found for square pillar structures with low values of s , while circular pillar arrays performed better for large s , with a crossover at $s \approx 0.15$. The Raman signal always arises from the edges of the cylinders, irrespective of the s value, and SERS enhancement from the intercylinder areas was not observed. This is an indication that detailed structural properties come into play. The difference in SERS localization might originate from the longer interaction length of the sides of the square prisms compared to cylindrical pillars, where the shortest intercylinder distance corresponds to only one point on the cylinder perimeter. The plasmon confinement between the square structures provide stronger local fields around their sharper edges (points of maximum curvature) in comparison to circular cylinders.

Note that although the quality of the replicated structures is nearly perfect, slightly rounded edges of the array structures

indicate a finite contact angle where the polymer has made contact with the surface of the patterned electrode during the EHL process. Apart from this small effect, the profile of the polymer square-shaped prisms is nearly rectangular (Figure 2a,b). Importantly, the edge radius that has a strong effect on the SERS enhancement is constant and reproducible across the entire substrate.

To understand the SERS response of EHL-structured substrates, the square pillar arrays were numerically simulated by a two-dimensional model (Figure 3d, I) of gold-coated EHL structures ($h = 500$ nm and Au thickness = 20 nm) using a finite-element method, where a plane wave is incident normal to the substrate with a linear polarization perpendicular to the top edge (see the Experimental Section for further details). This simulation of a square cross section is infinite in the second lateral direction (i.e., infinite ridges with square cross sections). The scattered electric field generated by the gold-coated structures in vacuum was simulated for various s ratios. While a three-dimensional model would provide more accurate simulations of EHL morphologies, they are computationally very intensive because of the micrometer-sized dimensions of the structures.

The results of the simulations in the inset II of Figure 3d show that the electric fields excited on the gold-coated structures increase with decreasing gap-to-width ratio s . While the periodic grating couples light into plasmon–polariton and propagating plasmon resonances by diffraction, these are not able to couple with each other if the gap between the structures is large. The coupling for small s leads to strong localization between the structures and consequently high fields (Figure 3d) and SERS enhancements in interstitial gaps. The increase in SERS upon a decrease of periodicity (gap distance) could also be due to resonant excitation of propagating plasmons diffractively coupled into the structure.

Although nonpolarized detection is the norm in SERS imaging, the EHL-generated substrates were also examined under horizontally and vertically polarized excitation illumination (Figure 4) using an AFM-coupled confocal scanning Raman microscope (Ntegra Spectra, NT-MDT). This reveals the interplay of polarization with surface topography in the SERS response. The confocal Rayleigh scattering image of a square pillar array in Figure 4b is similar to the AFM image (Figure 4a). Rayleigh scattering is dependent on the size of the scatterers, and hence, the large structures have a dominant signal in the image. Moreover, it indicates that plasmons scattered at the laser (excitation) wavelength are localized on the pillars. The SERS images of the periodic array of square prisms reveal a well-separated periodic distribution of the Raman intensity in between the prisms. The bright image regions of highest SERS intensity were reproducible across the substrate. The slightly increased intensity of the Raman spectra for vertically polarized illumination (Figure 4c) compared to horizontal polarization (Figure 4d) probably arises from minor variations in incident laser power for the two polarizing conditions (Figure 2a,b).

The observed dependence on illumination polarization confirms that large electromagnetic fields are localized in the interstitial space between adjacent microstructures. While incident radiation excites a plasmon trapped in this interstitial space, the polarization charges on either side of the gap oppose each other to produce high dipolar fields that couple to each other if the gap is sufficiently narrow, which is consistent with the observations of Figures 3 and 4. The coupling between plasmons on the pillars results in red-shifted gap (interstitial)

plasmons. The SERS signals that occur at these red-shifted wavelengths (SERS is Stokes shifted from the incident excitation) are therefore enhanced in the gap region. Such polarization-sensitive anisotropic localization of plasmons and SERS signals offers the possibility of switchable nanophotonic logic devices and multiplexed detection at the single structure level.

In conclusion, we have demonstrated an elegant approach for the manufacture of SERS-active architectures on the micrometer scale using EHL. The generated structures display plasmon-dependent phenomena that can be controlled by the EHL patterning process. Tailoring the structure of the gold-coated substrates allows tuning of the light–surface plasmon interactions and, hence, the SERS signal enhancement. Overall enhancement factors up to 1.0×10^7 were reproducibly obtained. The SERS enhancement depends on the geometry and the dimensions of the surface structures, parametrized by the ratio of the structure width to their spacing. The polarization-dependent surface-enhanced Raman scattering reveals the highest intensity at the interstitial locations of the periodic structures. The ability to carefully design highly reproducible periodic arrays enables the control of localized plasmonic fields for a variety of lab-on-chip sensing devices. The polarization effect presents an additional degree of freedom for the use of EHL-generated platforms for switchable nanophotonic devices and multiplexed SERS detection at the local microstructure level.

■ EXPERIMENTAL SECTION

Polystyrene ($M_w = 100$ kg mol⁻¹, $M_w/M_n < 1.07$) was purchased from Polymer Standards Service GmbH, Mainz, Germany. Toluene was purchased from Fisher Scientific and used as the main solvent. Highly polished p-doped silicon (Si) wafers with $\langle 100 \rangle$ crystal orientation (Wafernet GmbH, Eching, Germany) were used as substrates. Patterned silicon wafers were obtained from X-lith eXtreme Lithography, Ulm, Germany.

Films with varying thicknesses were generated by spin-coating onto silicon substrates from toluene solutions with typical concentrations of 2–3% polymer by weight. Prior to spin-coating, the substrates were cleaned in a “Piranha” solution consisting of 3:1 H₂SO₄ (98%)/H₂O₂ (30%), followed by thorough rinsing with deionized water and drying under nitrogen. Substrates as well as top electrodes were snow-jet cleaned immediately before film deposition and device assembly. A capacitor setup was assembled using the polymer-covered substrate as one of the electrodes. Topographically structured top electrodes were mounted facing the polymer-covered substrate, leaving a thin air gap, d (Figure 1). Silicon oxide colloids were used as spacers to adjust d . Both capacitor electrodes were electrically contacted using silver paint (Electrodag 1415M). The films were sequentially liquefied by thermal annealing, raising the temperature above the T_g of each resist, and a constant voltage of 80 V was applied across the two electrodes of the capacitor. The experiment was terminated by quenching the assembly to room temperature before removing the electric field. After quenching to room temperature, which induces the solidification of the polymer, the electric field was disconnected, and the upper electrode was removed.

The evolving patterns were observed with a standard optical microscope (Olympus BX 40) operated in clean-room conditions. A digital camera connected to the microscope was

read out by imaging software (Carl Zeiss Visiocam). A NanoScope IV Multimode Dimension 3100 AFM was used to quantitatively determine the sample topography. Height and phase images were analyzed using the Nanoscope software (Digital Instruments). The AFM measurements yielded the film thickness h , the plate spacing d , the characteristic wavelength λ , and the width and height (i.e., aspect ratios) of the generated patterns. Optical and AFM micrographs showed the lateral distribution of the patterned polymers on the substrate. The SEM measurements were performed using a LEO ULTRA 55 SEM including a Schottky emitter (ZrO/W cathode) at acceleration voltages of 5.0–10.0 kV with a lateral resolution of 2–5 nm. The EHL substrates were covered with a thin Au film using an Emitech sputter-coater with DC Ar plasma (gold target purity 99.999% supplied by Kurt J. Lesker Company). The gold was deposited to approximately 20 nm as per the calibration of the sputter-coater (current versus deposition rate). Accordingly, two cycles of 30 s at 70 mA were carried out. The deposition was performed onto all of the EHL-formed structures and onto polymer films as reference samples.

SERS measurements were carried out with an InVia Renishaw Raman Microscope System equipped with 633 and 785 nm lasers. The spectra were typically acquired with a 10 s exposure time and laser powers of 3 and 10 mW at the sample at 633 and 785 nm, respectively. SERS maps were acquired in Streamline mode (line scan) with a 20 s exposure time and 6 and 100 mW powers at 633 and 785 nm, respectively. A 50 \times objective with a numerical aperture of 0.75 was used for all measurements. Optical measurements were carried out with an Olympus BX51 microscope equipped with an incoherent white light (halogen) source and an optical fiber coupled to a QE65000 Ocean Optics spectrometer. The spectra were normalized with respect to those recorded on flat gold.

The SERS enhancement factor was calculated by comparing the intensities of the unenhanced Raman scattering (IRaman) peak at 1070 cm^{-1} of pure benzenethiol liquid obtained by focusing the laser into a quartz cell and the corresponding SERS signals. The detection volume of the solution-phase benzenethiol sample (V_f) was calculated using the following relation, $V_f = \text{depth of focus} \times \text{focus area} = (1.4n\lambda/\text{NA}^2) \times \pi(0.4\lambda/2\text{NA})^2$. The surface density of the adsorbed benzenethiol molecules on the surface was taken as $\rho_s = 3.3 \text{ molecules/nm}^2$ ¹⁸ and the enhanced area (A) was taken as the diffraction-limited spot size ($\pi(0.4\lambda/2\text{NA})^2$). The enhancement factor was thus obtained by the relation $\text{EF} = [I_{\text{SERS}}/(\rho_s A)]/[I_{\text{Raman}}/(\rho_s V_f)]$.

Numerical simulations were performed using a commercial finite element solver COMSOL v4.3. The illustration of the model is depicted in Figure 3d, I. The height of the simulated pillars was 0.5 μm , and the thickness of the gold layer was 20 nm. The structures were illuminated with a p-polarized plane wave traveling normal to the surface. Floquet periodicity boundary conditions were applied to the system. Wavelength-dependent optical constants of silicon and gold were taken from ref 19. The refractive index of the polymer was fixed at 1.58, and the surrounding medium was taken as 1. A curvature radius of 10 nm was applied at the upper edges of the rods. The electric field was calculated as a ratio of its value at a given point (1 nm away from the pillar edge) divided by the incident field, $|E|/|E_0|$. The SERS enhancement was calculated for the excitation wavelength and the measured Raman wavelength ($|E|_{633 \text{ nm}}/|E_0|$) $^2 \times (|E|_{680 \text{ nm}}/|E_0|)^2$.

ASSOCIATED CONTENT

Supporting Information

Further information regarding the structural analysis of the deposited gold film and the calculation of the enhancement factor is available. This material is available free of charge via the Internet at <http://pubs.acs.org>.

AUTHOR INFORMATION

Corresponding Authors

*E-mail: S.Mahajan@soton.ac.uk (S.M.).

*E-mail: p.goldbergoppenheimer@bham.ac.uk (P.G.O.).

Notes

The authors declare no competing financial interest.

ACKNOWLEDGMENTS

S.M. and U.S. acknowledge funding from EPSRC (EP/H028757/1, EP/H028757/2) and EP/G060649/1, respectively. We acknowledge I. Arkov (NT-MDT) for the assistance with acquiring the polarized SERS data. We appreciate the advice of J. J. Rickard regarding the SEM imaging.

REFERENCES

- (1) Barnes, W. L.; Dereux, A.; Ebbesen, T. W. Surface Plasmon Subwavelength Optics. *Nature* **2003**, *424*, 824–830.
- (2) Ozbay, E. Plasmonics: Merging Photonics and Electronics at Nanoscale Dimensions. *Science* **2006**, *311*, 189–193.
- (3) Tripp, R. A.; Dluhy, R. A.; Zhao, Y. Novel Nanostructures for SERS Biosensing. *Nano Today* **2008**, *3*, 31–37.
- (4) Patel, I. S.; Premasiri, W. R.; Moir, D. T.; Ziegler, L. D. Barcoding Bacterial Cells: A SERS-Based Methodology for Pathogen Identification. *J. Raman Spectrosc.* **2008**, *39*, 1660–1672.
- (5) Kneipp, K.; Wang, Y.; Kneipp, H.; Perelman, L. T.; Itzkan, I.; Dasari, R. R.; Feld, M. S. Single Molecule Detection Using Surface-Enhanced Raman Scattering (SERS). *Phys. Rev. Lett.* **1997**, *78*, 1667–1670.
- (6) Nie, S.; Emory, S. R. Probing Single Molecules and Single Nanoparticles by Surface-Enhanced Raman Scattering. *Science* **1997**, *275*, 1102–1106.
- (7) Morfa, A. J.; Rowlen, K. L.; Reilly, T. H., III; Romero, M. J.; van de Lagemaat, J. Plasmon-Enhanced Solar Energy Conversion in Organic Bulk Heterojunction Photovoltaics. *Appl. Phys. Lett.* **2008**, *92*, 013504.
- (8) Chou, S. Y.; Krauss, P. R.; Renstrom, P. J. Imprint Lithography with 25-Nanometer Resolution. *Science* **1996**, *272*, 85–87.
- (9) Chou, S. Y.; Zhuang, L.; Deshpande, P.; Chen, L.; Sun, X. Y. Lithographically Induced Self-Assembly of Periodic Micropillar Arrays in a Single Homopolymer Film. *Abstr Pap. Am. Chem. Soc.* **2000**, *219*, U405–U405 ; Part 2..
- (10) Menard, E.; Meitl, M. A.; Sun, Y. G.; Park, J. U.; Shir, D. J. L.; Nam, Y. S.; Jeon, S.; Rogers, J. A. Micro- and Nanopatterning Techniques for Organic Electronic and Optoelectronic Systems. *Chem. Rev.* **2007**, *107*, 1117–1160.
- (11) Qin, D.; Xia, Y. N.; Rogers, J. A.; Jackman, R. J.; Zhao, X. M.; Whitesides, G. M. *Microfabrication Microstructures and Microsystems*; Springer-Verlag: Berlin, Heidelberg, Germany, 1998; Vol. 194; pp 1–20.
- (12) Yan, B.; Thubagere, A.; Premasiri, W. R.; Ziegler, L. D.; Dal Negro, L.; Reinhard, B. M. Engineered SERS Substrates with Multiscale Signal Enhancement: Nanoparticle Cluster Arrays. *ACS Nano* **2009**, *3*, 1190–1202.
- (13) Goldberg-Oppenheimer, P.; Mahajan, S.; Steiner, U. Hierarchical Electrohydrodynamic Structures for Surface-Enhanced Raman Scattering. *Adv. Mater.* **2012**, *24*, OP175–OP180.
- (14) Netti, C.; Lincoln, J.; Flinn, G. Reliable Substrate Technology for Surface-Enhanced Raman Spectroscopy. *Raman Technology for Today's Spectroscopists* **2005**, *3*–8.

- (15) Etchegoin, P. G.; Le Ru, E. C. A Perspective on Single Molecule SERS: Current Status and Future Challenges. *Phys. Chem. Chem. Phys.* **2008**, *10*, 6079–6089.
- (16) Kahl, M.; Voges, E.; Kostrewa, S.; Viets, C.; Hill, W. Periodically Structured Metallic Substrates for SERS. *Sens. Actuators, B* **1998**, *51*, 285–291.
- (17) Joo, T. H.; Kim, M. S.; Kim, K. Surface-Enhanced Raman Scattering of Benzenethiol in Silver Sol. *J. Raman Spectrosc.* **1987**, *18*, 57–60.
- (18) Love, J. C.; Estroff, L. A.; Kriebel, J. K.; Nuzzo, R. G.; Whitesides, G. M. Self-Assembled Monolayers of Thiolates on Metals as a Form of Nanotechnology. *Chem. Rev.* **2005**, *105*, 1103–1170.
- (19) Ni, X.; Liu, Z.; Kildishev, A. V. *PhotonicsDB: Optical Constants*. <https://nanohub.org/resources/3692> (2008).